Influence of dipolar interactions on the magnetic susceptibility spectra of ferrofluids

Influence of dipolar interactions on the magnetic susceptibility spectra of ferrofluids

Julien O. Sindt

School of Chemistry, University of Edinburgh,

David Brewster Road, Edinburgh EH9 3FJ, Scotland

Philip J. Camp*

School of Chemistry, University of Edinburgh,

David Brewster Road, Edinburgh EH9 3FJ, Scotland and

Institute of Mathematics and Computer Sciences,

Ural Federal University, 51 Lenin Avenue, Ekaterinburg 620000, Russia

Sofia S. Kantorovich

Department of Computational Physics, University of Vienna,

Sensengasse 8/9, 1090 Vienna, Austria and

Institute of Mathematics and Computer Sciences,

Ural Federal University, 51 Lenin Avenue, Ekaterinburg 620000, Russia

Ekaterina A. Elfimova and Alexey O. Ivanov

Institute of Mathematics and Computer Sciences,

Ural Federal University, 51 Lenin Avenue, Ekaterinburg 620000, Russia

(Dated: June 7, 2016)

Abstract

The frequency-dependent magnetic susceptibility of a ferrofluid is calculated under the assumption that the constituent particles undergo Brownian relaxation only. Brownian-dynamics simulations are carried out in order to test the predictions of a recent theory [A. O. Ivanov *et al.*, Soft Matter **12**, 3507 (2016)] that includes the effects of interparticle dipole-dipole interactions. The theory is based on the so-called modified mean-field approach, and possesses the following important characteristics: in the low-concentration, non-interacting regime, it gives the correct single-particle Debye-theory results; it yields the exact leading-order results in the zero-frequency limit; it includes particle polydispersity correctly from the outset; and it is based on firm theoretical foundations allowing, in principle, systematic extensions to treat stronger interactions and/or higher concentrations. The theory and simulations are compared in the case of a model monodisperse ferrofluid, where the effects of interactions are predicted to be more pronounced than in a polydisperse ferrofluid. The susceptibility spectra are analyzed in detail in terms of the low-frequency behavior, the position of the peak in the imaginary (out-of-phase) part, and the characteristic decay time of the magnetization autocorrelation function. It is demonstrated that the theory correctly predicts the trends in all of these properties with increasing concentration and dipolar coupling constant, the product of which is proportional to the Langevin susceptibility χ_{L}. The theory is in quantitative agreement with the simulation results as long as $\chi_{\mathrm{L}} \lesssim 1$.

PACS numbers: 47.65.Cb, 75.50.Mm, 75.30.Cr, 05.10.Gg

*Corresponding author: philip.camp@ed.ac.uk

I. INTRODUCTION

Ferrofluids are colloidal suspensions of magnetized and sterically stabilized nanoparticles dispersed in a non-magnetic carrier liquid [1]. The magnetic susceptibility is a key property of ferrofluids, determining the response of the magnetization M to an applied field H. The initial static magnetic susceptibility $\chi = \partial M/\partial H|_{H=0}$ and the full magnetization curve $M(H)$ of magnetic materials have been the subjects of intense theoretical and experimental study since the early 1900s, when Langevin's theory of an ideal (non-interacting) paramagnet was proposed [2]. In the case of ferrofluids, a vast range of models has been developed to link the macroscopic magnetic response to the granulometric composition of the ferrofluid and the interactions between the magnetic nanoparticles. Examples include Weiss' mean-field theory [3, 4], the mean-spherical approximation closure of the Ornstein-Zernike equation [5, 6] the high-temperature approximation [7, 8], first-order [9] and second-order modified mean-field (MMF) theories [10, 11], and Born-Mayer cluster-expansion theories [12–14]. As judged from comparisons with experimental and computer-simulation data, the most successful systematic approach to the magnetic response of ferrofluids is the MMF theory. Although first proposed as an *ad-hoc* modification of the Weiss mean-field theory [9], the MMF approach arises naturally from a rigorous application of the Yvon-Born-Bogolyubov-Green-Kirkwood hierarchy [15] linking the one-particle distribution function to the two-particle correlation function [10, 11]. In physical terms, the MMF provides a means of including the effective field experienced by a particle due to the external field and all of the other particles. By approximating the pair-correlation function in various ways, e.g., through virial-type expansions and thermodynamic perturbation theory, a systematic approach to χ and $M(H)$ can be established. The first-order MMF (MMF1) theory gives the exact leading-order correction to the Langevin theory, which is proportional to the square of the Langevin susceptibility. The MMF theory at various levels of approximation, and almost all other available theories, have been tested critically against experimental data and computer-simulation results for monodisperse and polydisperse magnetite ferrofluids over broad ranges of temperature and concentration [10, 11, 16–18]. In Ref. 16, for example, it was shown that the second-order MMF theory (required for concentrated ferrofluids) is the only available approach that gives a consistent link between the particle-size distribution and $M(H)$ over all concentrations. It is worth pointing out that theories of the initial magnetic susceptibility

are trivially applied to static dielectric constants of polar molecular materials.

The frequency-dependent magnetic susceptibility $\chi(\omega) = \chi'(\omega) + i\chi''(\omega)$ is an important property of soft magnetic materials [19, 20] that forms the basis of many applications [21–25]. For instance, the heating of a magnetic fluid with an AC magnetic field is proportional to the imaginary (out-of-phase) part $\chi''(\omega)$ [26]. This has led to applications in medicine [27, 28], such as localized heating (hyperthermia) and destruction of diseased tissue [29–31]. In the linear-response (weak-field) regime, the susceptibility spectrum $\chi(\omega)$ is related to the decay of spontaneous magnetization fluctuations in zero field [15]. The dynamics of this process depends sensitively on the particle size [1]: the relaxation time from the Néel mechanism (fluctuation within the crystal structure of the nanoparticle) increases exponentially with the nanoparticle volume, while the Brownian relaxation time (arising from body rotation) increases linearly with the volume. In small magnetite particles, with diameters of less than 10 nm, the Néel mechanism dominates with relaxation times on the order of $\tau_{\rm N} \sim 1$ ns. In larger magnetite particles, with diameters of more than 10 nm, the Brownian mechanism dominates with relaxation times on the order of $\tau_{\rm B} \sim 1$–100 μs. The dynamical analogue of the Langevin theory is the celebrated Debye theory, widely applied to both magnetic and electric polar materials [32, 33]. The Debye theory applies when the particles are essentially non-interacting, i.e., in an ideal paramagnet or ideal polar gas, and the zero-frequency limit of the Debye theory gives the Langevin susceptibility.

Interparticle dipole-dipole interactions do not affect the Néel mechanism significantly, but they do slow down the Brownian mechanism. It goes without saying that it is vital to understand the effects of material parameters on such processes in order to develop new materials for applications, such as hyperthermia [34–36]. Several attempts have been made to describe the effects of interparticle interactions on the susceptibility spectrum [37–40]. In all cases, dipole-dipole interactions are predicted to increase the Brownian relaxation times, and hence decrease the peak (absorption) frequency in $\chi''(\omega)$. In physical terms, strong positional and orientational correlations between particles mean that there are collective cluster-type motions, which are slower than single-particle motions. Such effects have been detected in experiments [41–43] although the analysis is complicated because both the interactions and the polydispersity of the sample must be taken in to account.

Recently, a new dynamical theory of interacting dipolar particles in the Brownian-relaxation regime has been proposed that is analogous to the first-order MMF approach

outlined above [44]. The theory has the following essential properties: firstly, the correct single-particle Debye-theory results are recovered in the limit of low concentration and/or vanishing interactions; secondly, in the zero-frequency limit, the theory recovers the correct MMF1 result for the static susceptibility (for any particle-size distribution); thirdly, the particle-size distribution is prescribed at the outset, and so there is no need for *ad-hoc* generalizations of a simple single-particle picture to the polydisperse case; and finally, the theory is based on rigorous statistical-mechanical principles, and so it should be possible to extend it systematically to higher orders in concentration and dipolar coupling constant. The dynamical version of the MMF1 theory (referred to here simply as the MMF1 theory) has been used to analyze various features of the susceptibility spectra in real polydisperse ferrofluids [20], namely, the behaviors of χ' and χ'' in the low-frequency domain, and the peak (absorption) frequency of χ'' [44]. The analysis showed that the susceptibility spectrum is not a simple superposition of single-particle, Debye-theory functions; it is a more complex function that depends not only on the particle-size distribution, but also on the strengths of the interactions and the overall concentration. For instance, in polydisperse systems, the peak frequency is much less sensitive to increasing concentration than in monodisperse systems. This is due to the peak frequency of a polydisperse ferrofluid being dominated by a small fraction of large particles, and the interactions between these particles are only weakly affected by a change in overall concentration; in a monodisperse ferrofluid, all particles contribute equally to the response and are affected by concentration to the same extent. Note that the models discussed here are not necessarily applicable to polar molecular materials, because the relaxation of electric polarization fluctuations over short timescales are inertial rather than Brownian. Hence, Brownian models will always be approximations to the true molecular motions.

The dynamical MMF1 theory has not yet been tested rigorously against accurate computer-simulation results. This is the aim of the current work. To maximize the effects of particle interactions and concentration on the susceptibility spectrum, the study will be restricted to the monodisperse case. Brownian dynamics (BD) simulations will be used to compute the susceptibility spectra, and the key characteristics will be extracted and compared to the predictions of the Debye and MMF1 theories. It will be demonstrated that the MMF1 does indeed predict all of the right trends in the spectral properties, and that the agreement between theory and simulation is quantitative in the weak-interaction

regime. The rest of this article is organized as follows. In Section II, the monodisperse ferrofluid model is defined (II A), the Debye and MMF1 theories are summarized (II B and II C, respectively), some essential elements of linear-response theory are noted (II D), and the details of the BD simulations are explained (II E). The results are presented in Section III, and Section IV concludes the paper.

II. MODEL, THEORY, AND SIMULATIONS

A. Model

The system is comprised of N dipolar particles of mass m in a three-dimensional volume V at temperature T. The total interaction potential between particles i and j is $u_{ij} = u_{ij}^{\mathrm{WCA}} + u_{ij}^{\mathrm{d}}$, a sum of the short-range Weeks-Chandler-Andersen (WCA) potential and the long-range dipolar (d) potential. The WCA potential is

$$u_{ij}^{\mathrm{WCA}} = \begin{cases} 4\epsilon\left[\left(\dfrac{\sigma}{r_{ij}}\right)^{12} - \left(\dfrac{\sigma}{r_{ij}}\right)^{6}\right] + \epsilon & r_{ij} \le r_{\min} \\ 0 & r_{ij} > r_{\min} \end{cases} \tag{1}$$

where $r_{ij} = |\boldsymbol{r}_{ij}|$ is the separation between the particles, $r_{\min} = 2^{1/6}\sigma$ is the minimum in the Lennard-Jones (LJ) potential, and ϵ and σ are the LJ energy and range parameters, respectively. The magnetic dipolar interaction is

$$u_{ij}^{\mathrm{d}} = \frac{\mu_0}{4\pi}\left[\frac{(\boldsymbol{\mu}_i \cdot \boldsymbol{\mu}_j)}{r_{ij}^3} - \frac{3(\boldsymbol{\mu}_i \cdot \boldsymbol{r}_{ij})(\boldsymbol{\mu}_j \cdot \boldsymbol{r}_{ij})}{r_{ij}^5}\right] \tag{2}$$

where $\boldsymbol{\mu}_i$ is the dipole moment on particle i, and μ_0 is the vacuum magnetic permeability. As usual, reduced units are employed: the reduced concentration is $\rho^* = \rho\sigma^3$ where $\rho = N/V$; the reduced dipole moment is $\mu^* = \sqrt{\mu_0\mu^2/4\pi\sigma^3\epsilon}$; the reduced temperature is $T^* = k_{\mathrm{B}}T/\epsilon$; the dipolar coupling constant is $\lambda = (\mu^*)^2/T^*$; and the time is measured in units of $\tau_{\mathrm{LJ}} = \sqrt{m\sigma^2/\epsilon}$.

B. Debye theory

The Debye theory of polar relaxation is well known [32, 33], but the basic elements of the theory are outlined here in order to enable straightforward extensions to the MMF1

case in Section II C. The particles are modeled as undergoing Brownian motion in a solvent with shear viscosity η. The single-particle (or non-interacting particle) translational and rotational diffusion constants are given by the Stokes-Einstein(-Debye) relations

$$D_{\text{trans}} = \frac{k_{\text{B}}T}{3\pi\eta\sigma} \tag{3}$$

$$D_{\text{rot}} = \frac{k_{\text{B}}T}{\pi\eta\sigma^3}. \tag{4}$$

The interaction energy U between a particle dipole $\boldsymbol{\mu}$ and an AC field $H_z(t) = he^{-i\omega t}$ linearly polarized in the laboratory z direction is

$$\frac{U}{k_{\text{B}}T} = -(\alpha\cos\theta)e^{-i\omega t} \tag{5}$$

where $\alpha = \mu_0\mu h/k_{\text{B}}T$ is the Langevin interaction parameter, and θ is the polar angle of the dipole orientation vector. The rotational motion of a single particle is described by the probability density $W(\theta, t)$ which is the solution of the Fokker-Planck equation [45, 46]

$$\frac{1}{D_{\text{rot}}}\frac{\partial W}{\partial t} = \frac{1}{\sin\theta}\frac{\partial}{\partial\theta}\left[\sin\theta\left(\frac{\partial W}{\partial\theta} + \frac{W}{k_{\text{B}}T}\frac{\partial U}{\partial\theta}\right)\right]. \tag{6}$$

The equilibrium probability density satisfies the equation $\partial W/\partial\theta + (W/k_{\text{B}}T)\partial U/\partial\theta = 0$ and is given by $W_0 = C\exp(\alpha\cos\theta)$ where C is a normalization factor. In the linear-response regime, where α is a small parameter and only linear terms are retained, the time-dependent solution of Eq. (6) is of the form $W = 1 + (\alpha\cos\theta)f(\omega)e^{-i\omega t}$. A straightforward calculation gives $f(\omega) = (1 - i\omega\tau_{\text{B}})^{-1}$ and

$$W = 1 + (\alpha\cos\theta)\left(\frac{1}{1 - i\omega\tau_{\text{B}}}\right)e^{-i\omega t} \tag{7}$$

where the Brownian rotation time is

$$\tau_{\text{B}} = \frac{1}{2D_{\text{rot}}}. \tag{8}$$

The magnetization in the z direction is

$$M_z(t) = \frac{\rho\mu}{2}\int_{-1}^{1} W\cos\theta\ \mathrm{d}\cos\theta = \left(\frac{\chi_{\text{L}}}{1 - i\omega\tau_{\text{B}}}\right)H_z(t) \tag{9}$$

where

$$\chi_{\text{L}} = \frac{\rho\mu_0\mu^2}{3k_{\text{B}}T} = \frac{4\pi\rho^*\lambda}{3} \tag{10}$$

is the Langevin static susceptibility. The frequency-dependent susceptibility in the Debye theory is therefore

$$\chi_{\rm D}(\omega) \;=\; \left(\frac{\chi_{\rm L}}{1-i\omega\tau_{\rm B}}\right) = \chi'_{\rm D}(\omega) + i\chi''_{\rm D}(\omega) \tag{11a}$$

$$\chi'_{\rm D}(\omega) \;=\; \frac{\chi_{\rm L}}{1+(\omega\tau_{\rm B})^2} \tag{11b}$$

$$\chi''_{\rm D}(\omega) \;=\; \frac{\chi_{\rm L}\omega\tau_{\rm B}}{1+(\omega\tau_{\rm B})^2}. \tag{11c}$$

The peak frequency in $\chi''_{\rm D}(\omega)$ is $\omega_0 = \tau_{\rm B}^{-1}$. The leading-order deviations from the zero-frequency values $\chi'_{\rm D}(0) = \chi_{\rm L}$ and $\chi''_{\rm D}(0) = 0$ are proportional to ω^2 and ω, respectively.

$$\chi'_{\rm D}(\omega) \;\approx\; \chi_{\rm L}\left[1-(\omega\tau_{\rm B})^2\right] \tag{12}$$

$$\chi''_{\rm D}(\omega) \;\approx\; \chi_{\rm L}\omega\tau_{\rm B} \tag{13}$$

C. First-order modified mean-field theory

The modified mean-field theories [10, 11] revolve around determining the one-particle probability density based on its connection to the pair-correlation function (PCF) through the Yvon-Born-Bogolyubov-Green-Kirkwood hierarchy [15]. In physical terms, the one-particle probability density (and hence the magnetization) is determined not by the applied field, but by an effective field containing contributions from all of the other particles which are represented by the PCF. In seeking a systematic approach to this effective field, the pair-correlation function is expanded in powers of ρ and λ. The MMF1 theory corresponds to keeping the leading-order term proportional to $\rho\lambda$. The case of a static applied field was treated at both first-order and second-order levels in Refs. 10 and 11. In Ref. 44 it was shown that in the presence of an applied AC field, the effective interaction energy between a single particle and the effective AC field at the MMF1 level is

$$\frac{U_{\rm eff}}{k_{\rm B}T} = -(\alpha\cos\theta)e^{-i\omega t}\left[1+\frac{1}{3}\chi_{\rm D}(\omega)\right] \tag{14}$$

which mirrors the static case, where the effective field is increased by a factor of $(1+\chi_{\rm L}/3)$ [10, 11]. By once again seeking a solution of the Fokker-Planck equation of the form $W = 1+(\alpha\cos\theta)f(\omega)e^{-i\omega t}$, but with $U_{\rm eff}$ in place of U, the function $f(\omega)$, the magnetization, and the susceptibility spectrum can be determined straightforwardly just as in Section II B.

The key results are that $f(\omega) = [1 + \chi_{\rm D}(\omega)/3](1 - i\omega\tau_{\rm B})^{-1}$ and, following Eq. (9),

$$\chi(\omega) \;=\; \chi'(\omega) + i\chi''(\omega) \tag{15a}$$

$$\chi'(\omega) \;=\; \chi'_{\rm D}(\omega) + \frac{1}{3}\left\{[\chi'_{\rm D}(\omega)]^2 - [\chi''_{\rm D}(\omega)]^2\right\} \tag{15b}$$

$$\chi''(\omega) \;=\; \chi''_{\rm D}(\omega)\left[1 + \frac{2}{3}\chi'_{\rm D}(\omega)\right]. \tag{15c}$$

The static susceptibility is

$$\chi(0) = \chi_{\rm L}\left(1 + \frac{1}{3}\chi_{\rm L}\right) \tag{16}$$

which corresponds to the MMF1 and high-temperature approximation results [7–11]. The peak frequency in $\chi''(\omega)$ is given by

$$\omega_0 = \tau_{\rm B}^{-1}\left[-\chi_{\rm L} + \left(1 + \frac{2}{3}\chi_{\rm L} + \chi_{\rm L}^2\right)^{1/2}\right]^{1/2} \approx \tau_{\rm B}^{-1}\left(1 - \frac{1}{3}\chi_{\rm L}\right). \tag{17}$$

This shows that increasing the concentration and/or dipolar coupling constant leads to a reduction in peak frequency, reflecting stronger orientational correlations between particles and the growth of collective orientational dynamics. The low-frequency behaviors of the real and imaginary parts of $\chi(\omega)$ are

$$\chi'(\omega) \;\approx\; \chi(0)\left[1 - A(\omega\tau_{\rm B})^2\right] \tag{18}$$

$$\chi''(\omega) \;\approx\; B\chi_{\rm L}\omega\tau_{\rm B} \tag{19}$$

where

$$A \;=\; \frac{3 + 3\chi_{\rm L}}{3 + \chi_{\rm L}} \approx 1 + \frac{2}{3}\chi_{\rm L} \tag{20}$$

$$B \;=\; 1 + \frac{2}{3}\chi_{\rm L}. \tag{21}$$

D. Linear-response theory

In linear-response theory, the susceptibility spectrum can also be expressed in terms of the equilibrium (zero-field) magnetization autocorrelation function (MACF) $C(t)$ [15]. For an infinitely thin sample oriented along the laboratory z axis (as is assumed in theory [10, 11, 44]) or for a sample surrounded by a perfect conductor (as is assumed in simulations – see Section II E) the demagnetization fields vanish. In this case, the susceptibility spectrum is given by

$$\chi(\omega) = \chi(0)\left[1 + i\omega\int_0^\infty C(t)e^{i\omega t}\,{\rm d}t\right] \tag{22}$$

where the static susceptibility is

$$\chi(0) = \frac{\mu_0 \langle \boldsymbol{M}^2 \rangle}{3Vk_{\mathrm{B}}T}. \tag{23}$$

The MACF is defined by

$$C(t) = \frac{\langle \boldsymbol{M}(t) \cdot \boldsymbol{M}(0) \rangle}{\langle \boldsymbol{M}^2 \rangle} \tag{24}$$

where

$$\boldsymbol{M}(t) = \frac{1}{V} \sum_{i=1}^{N} \boldsymbol{\mu}_i(t) \tag{25}$$

is the instantaneous magnetization. Using these relations, it is possible to define, in general, a characteristic decay time for the MACF by

$$\tau_0 = \int_0^\infty C(t)\ \mathrm{d}t = \lim_{\omega \to 0} \left\{ \frac{1}{i\omega} \left[\frac{\chi(\omega)}{\chi(0)} - 1 \right] \right\} = \frac{B\chi_{\mathrm{L}}\tau_{\mathrm{B}}}{\chi(0)}. \tag{26}$$

In the Debye theory, $\tau_0 = \tau_{\mathrm{B}}$ and $C(t) = \exp\left(-t/\tau_{\mathrm{B}}\right)$. In the MMF1 theory

$$\tau_0 = \left(\frac{3 + 2\chi_{\mathrm{L}}}{3 + \chi_{\mathrm{L}}} \right) \tau_{\mathrm{B}} \approx \left(1 + \frac{1}{3}\chi_{\mathrm{L}} \right) \tau_{\mathrm{B}} \tag{27}$$

which increases with increasing concentration and dipolar coupling constant, reflecting a growth in collective orientational dynamics.

E. Simulations

Brownian dynamics (BD) simulations were performed using LAMMPS [47, 48]. The simulation cell was a three-dimensional cubic box with periodic boundary conditions applied. The reduced temperature was set equal to $T^* = 1$ in all cases. Densities ρ^* and dipolar coupling constants λ were chosen to span a range of Langevin susceptibilities up to $\chi_{\mathrm{L}} = 2.93$: one set was run with $\rho^* = 0.20$ and $0.25 \leq \lambda \leq 3.50$; and another set with $\lambda = 1$ and $0.10 \leq \rho^* \leq 0.70$. The system parameters are summarized in Table I. Note that $\lambda \simeq 1$ and volume fraction $\varphi = \pi\rho^*/6 \simeq 0.1$ are typical values for real ferrofluids. Simulations at concentration $\rho^* = 0.20$ were also run with the dipole-dipole interactions switched off ($u_{ij}^{\mathrm{d}} = 0$, corresponding to the Debye theory of non-interacting particles) in order to check the simulation and analysis protocols. In order to calculate accurate MACFs, it was necessary to simulate very long trajectories, and therefore quite small systems with $N = 216$ particles were chosen. To assess finite-size effects, some larger systems with $N = 512$ particles were run with the highest dipolar coupling constants ($\rho^* = 0.2$, $\lambda = 3.00$ and 3.50) and

at the highest densities ($\lambda = 1$, $\rho^* = 0.60$ and 0.70). The structural correlation lengths as compared to the box dimensions will be largest in these regimes, and so if finite-size effects are small here, they will also be small with smaller dipolar coupling constants and at lower densities. Long-range interactions were handled using the Ewald sum with conducting boundary conditions. To approximate BD, molecular-dynamics (MD) calculations were performed in the canonical (NVT) ensemble using a Langevin thermostat with a Stokes-force friction coefficient γ that was sufficiently high to suppress inertial motion, but not so high that it made the Brownian translation and rotation times too long. The friction coefficient is related to the translation and rotational diffusion coefficients by $\gamma = k_{\mathrm{B}}T/mD_{\mathrm{trans}}$ and $\gamma = 3k_{\mathrm{B}}T/mD_{\mathrm{rot}}\sigma^2$, respectively. Using Eq. (8) the relationship between the Brownian rotation time and the friction coefficient is $\tau_{\mathrm{B}} = \gamma m\sigma^2/6k_{\mathrm{B}}T$. The moment of inertia of a particle was set equal to $I = m\sigma^2/10$, corresponding to a solid sphere of uniform mass density. The equations of motion were integrated using the velocity-Verlet algorithm with a reduced timestep $\delta t^* = 0.002$. From some test runs with non-interacting particles, the choice $\gamma^* = 20$ (equivalent to the LAMMPS damping time $\tau^*_{\mathrm{damp}} = 0.05$) was found to generate the correct MACF $[C(t) = \exp(-t/\tau_{\mathrm{B}})]$ and Brownian rotation time $\tau^*_{\mathrm{B}} = \gamma^*/6T^* = 10/3 = 1667\delta t^*$. Each simulation consisted of an equilibration stage of 2×10^6 timesteps, followed by a production of run of either 2×10^7 or 4×10^7 timesteps for non-interacting or interacting particles, respectively. Instantaneous configurations were output at intervals of 5 timesteps, from which the MACFs were computed. The Fourier transform of the MACF in Eq. (22) was carried out numerically without any filtering or windowing.

III. RESULTS

In order to validate the BD simulation methodology and analysis, simulations were first run at concentration $\rho^* = 0.20$ and with the dipole-dipole interactions turned off ($u^{\mathrm{d}}_{ij} = 0$) so that the dipole dynamics were governed solely by Brownian motion as dictated by the Langevin thermostat. No finite-size effects are anticipated here because the particle dipoles are not interacting with one another. The susceptibility spectra of six simulated systems with $0.50 \leq \lambda \leq 3.00$ are shown in Fig. 1 along with the Debye-theory results from Eq. (11). The agreement between simulation and theory is perfect without any fitting or scaling. If χ_{L} and τ_{B} in the Debye-theory expressions are treated as fitting parameters, then the fitted values

deviate from the theoretical values by only 0.07% and 0.1%, respectively. These results show that the system size, run duration, and numerical post-processing are all sufficient to obtain reliable results.

Figure 2 shows the static susceptibility calculated using Eq. (23) for each system with interactions. The simulation results with $N = 216$ and 512 particles are practically the same, and all are compared with the Langevin [Eq. (10)] and MMF1 [Eq. (16)] predictions. The MMF1 theory is accurate over the full range of $\chi_{\rm L}$ with a fixed value of $\lambda = 1$, while it is only accurate with $\chi_{\rm L} \leq 1.68$ ($\lambda \leq 2.00$) at a fixed value of $\rho^* = 0.20$. The reason for this difference is that the MMF1 result arises from an expansion that contains terms of order $\rho\lambda$ and $(\rho\lambda)^2$. The next terms of order $(\rho\lambda)^3$ give the second-order MMF (MMF2) result [10, 11]

$$\chi(0) = \chi_{\rm L}\left(1 + \frac{1}{3}\chi_{\rm L} + \frac{1}{144}\chi_{\rm L}^2\right) \tag{28}$$

which is also shown in Fig. 2. This does marginally better than MMF1, but it's clear that higher-order terms in λ are required. In fact, for a system with specified short-range interactions, the static susceptibility can be expressed as a combined virial expansion in ρ and thermodynamic-perturbation expansion in λ [10–14]. The correction of order $\rho^2\lambda^4$ is known, and the extension of the MMF2 expression to WCA particles at $T^* = 1$ is

$$\chi(0) = \chi_{\rm L}\left[1 + \frac{1}{3}\chi_{\rm L}\left(1 + \frac{0.943\lambda^2}{25}\right) + \frac{1}{144}\chi_{\rm L}^2\right]. \tag{29}$$

This is shown in Fig. 2 as 'MMF2 + $\rho^2\lambda^4$' plotted for the two cases of $\rho^* = 0.20$ and $\lambda = 1$. There is not much change from the MMF1 and MMF2 results for $\lambda = 1$, but the agreement with simulations at $\rho^* = 0.20$ is excellent, despite the short-range interactions being WCA and not hard sphere. This discussion is only meant to highlight the effects of truncating the expression for the static susceptibility at different orders. At present, the corresponding results for the susceptibility spectrum are known only at the MMF1 level. At this level of approximation, the properties should depend only on $\chi_{\rm L}$, and not on the particular values of ρ^* and λ. Figure 2 shows that this rule is obeyed up to $\chi_{\rm L} \simeq 1$, and above this point the different levels of approximation, and different choices of parameters, give different results. It is therefore anticipated that the dynamical version of MMF1 will be accurate as long as $\chi_{\rm L} \lesssim 1$.

Figure 3 shows the susceptibility spectra of interacting particles at concentration $\rho^* = 0.20$ from simulations, Debye theory, and MMF1 theory. The simulation results with $N =$

216 and 512 particles at $\lambda = 3.00$ are indistinguishable on the scale of the graph [Fig. 3(f)]. The simulation results show that the static susceptibility $\chi(0)$ is higher than the Langevin prediction, and that the peak frequency ω_0 decreases with increasing λ and $\chi_{\rm L}$. For systems with Langevin susceptibilities $\chi_{\rm L} \leq 1.26$, the agreement between simulation and MMF1 theory is good. For systems with $\chi_{\rm L} \geq 1.68$, there are substantial deviations between the observed and predicted peak frequencies and static susceptibilities.

The static-susceptibility results in Fig. 2 suggest that the MMF1-level theory should be more reliable for systems with $\lambda = 1$, and this is borne out by the susceptibility spectra shown in Fig. 4 for systems at $0.10 \leq \rho^* \leq 0.60$. For each value of $\chi_{\rm L}$ the differences between the simulated and theoretical results are smaller than those for the equivalent system at $\rho^* = 0.20$. Note that the simulation results with $N = 216$ and 512 particles at $\rho^* = 0.60$ are indistinguishable on the scale of the graph [Fig. 4(f)].

The peak frequencies in the simulated spectra were estimated by fitting functions of the same form as $\chi''_{\rm D}(\omega)$ [Eq. (11c)] to the tops of the peaks, and then compared to the theoretical predictions in Eq. (17). Examples of fits for two cases with $\chi_{\rm L} = 2.93$ ($\rho^* = 0.20$, $\lambda = 3.50$ and $\rho^* = 0.70$, $\lambda = 1$) are shown in Fig. 5(a); both systems contained $N = 216$ particles. The fitted peak positions do not depend significantly on the choice of fitting function (MMF1-type function, Gaussian, etc.). The fit parameters are shown in Table I, which also includes the spot checks with larger systems of $N = 512$ particles. All values are quoted to three significant figures, and the estimated uncertainties arising from the fitting are zero at this level of precision. Any scatter of the points is therefore due to statistical errors, which have not been estimated due to the time it would take to repeat the simulations a sufficient number of times.

The fitted parameters are plotted in Figure 6, along with the predictions from Debye theory and the MMF1 theory (both the full and linearized equations). Figure 6(a) shows that the peak frequency ω_0 decreases monotonically with increasing $\chi_{\rm L}$ reflecting the growing importance of collective orientational dynamics. Even so, the simulation results are not sensitive to system size: calculations with $N = 216$ and 512 particles with the highest dipolar coupling constants and at the highest densities are in excellent agreement. In the range $\chi_{\rm L} \lesssim 1$, both sets of simulation results (at $\rho^* = 0.20$ and with $\lambda = 1$) coincide. Although the full MMF1 curve deviates from the simulation results early on, the initial linear extrapolation is accurate up to $\chi_{\rm L} \simeq 1$. The MMF1 approach includes only the

leading-order correction to the susceptibility of order $|\chi_{\rm D}|^2$, and therefore it can be argued that quantities relative to the Debye theory should only be quoted to linear order in $\chi_{\rm L}$. With increasing $\chi_{\rm L}$, the simulation results and MMF1 theory diverge from one another. Above $\chi_{\rm L} \simeq 1$ the MMF1 theory tracks the results at $\rho^* = 0.20$, but this is accidental: the static-susceptibility results in Fig. 2 show that the MMF1 theory is not accurate with strong interactions.

The coefficients A and B in the low-frequency expansions of $\chi'(\omega)/\chi(0)$ ($\omega\tau_{\rm B} \leq 0.02$) and $\chi''(\omega)$ ($\omega\tau_{\rm B} \leq 0.004$) were determined from fits of the type shown in Fig. 5(b) and (c). The coefficients are plotted in Fig. 6(b) and (c), which show that with $\chi_{\rm L} \lesssim 1$, the results are practically the same in both systems at $\rho^* = 0.20$ and with $\lambda = 1$. Beyond this point, there are significant differences between the two sets of results, as was anticipated from the discussion of the static susceptibility. As for the peak frequency, the MMF1 theory and its initial linear extrapolation are close to both sets of simulation results up to $\chi_{\rm L} \simeq 1$, and above this point simulation and theory diverge. For these parameters, the simulation results are sensitive to system size only in the extreme cases of $\lambda = 3.50$ and $\rho^* = 0.70$. Since A and B reflect the lowest-frequency, longest length-scale motions, finite-size effects will be most pronounced in these cases. The characteristic decay time τ_0 is derived from the fitted values of B and $\chi(0)$, and is shown in Fig. 6(d). Once again, the MMF1 theory and its initial linear extrapolation are accurate up to $\chi_{\rm L} \simeq 1$, and then they diverge from the simulation results. Moreover, above this point, the two sets of simulations results no longer coincide. Since τ_0 depends on B, finite-size effects are observed, but only in the most extreme cases of $\lambda = 3.50$ and $\rho^* = 0.70$.

In general, the simulation results at $\rho^* = 0.20$ and $\lambda = 1$ are in good agreement as long as $\chi_{\rm L} \lesssim 1$. With higher values of $\chi_{\rm L}$, the simulations at $\rho^* = 0.20$ show higher static susceptibilities, lower peak frequencies in $\chi''(\omega)$, steeper gradients in $\chi(\omega)$ in the low-frequency regime, and longer characteristic decay times of the MACF, all arising from strong orientational correlations and collective dynamics with increasing values of λ. To complete the analysis, it is worth comparing the normalized susceptibility spectra $\chi(\omega)/\chi(0)$ for all simulated systems (containing $N = 216$ particles) and from the MMF1 theory, in order to isolate the changes in frequencies with increasing concentration and dipolar coupling constant. The results are shown in Fig. 7. This shows the extent to which the MMF1 theory gives a good description of the simulations with $\lambda = 1$, but deviates significantly

when λ is greater than this value.

Overall, the simulation results with $\chi_{\rm L} \lesssim 1$ are not dependent on the particular choices of ρ^* and λ, and hence this represents an 'MMF1' regime where the leading-order corrections to the Langevin and Debye theories are accounted for correctly in the MMF1 theory. At higher values of $\chi_{\rm L}$, the systems simulated at ρ^* exhibit dynamical properties that deviate from the MMF1 predictions, and from the simulated properties with $\lambda = 1$. Hence, there is a consistency between the static and dynamic magnetic responses of ferrofluids, in that higher-order terms in $\rho\lambda$ and especially λ are probably required to describe the properties of systems at fixed concentration and with high values of λ.

IV. CONCLUSIONS

A critical comparison was made between a new dynamical theory for the magnetic susceptibility spectrum of a monodisperse ferrofluid governed by Brownian relaxation and with significant interparticle dipole-dipole interactions, and numerical results obtained from Brownian-dynamics simulations. The theory is based on a rigorous statistical-mechanical approach, analogous to the modified mean-field theory of the static magnetization curve. Consequently, the theory recovers the exact leading-order correction to the Langevin static susceptibility in the zero-frequency limit, and gives the simple Debye-theory results in the non-interacting regime. In addition, the particle-size distribution is accounted for correctly in the theory, although this was not the focus of the current work. Instead, it was shown how various features of the susceptibility spectrum of a monodisperse ferrofluid depend on the concentration and dipolar coupling constant. These features are the low-frequency behaviors of the real and imaginary parts of the spectrum, the peak position in the imaginary part, and the characteristic timescale for relaxation of the magnetization autocorrelation function. On all counts, the theory was shown to be quantitatively accurate as long as the corresponding Langevin susceptibility $\chi_{\rm L} \lesssim 1$. The overall trends with stronger interactions are still accounted for correctly by the theory, but it is clear that higher-order corrections are required. With very high dipolar coupling constants in the range $\lambda \gtrsim 4$, the formation of long-lived dipolar chains and rings [49–51] should lead to a reduction in the peak frequency and a broadening of the susceptibility spectrum. Since the theory is based on a systematic statistical-mechanical approach, it is hoped that its extensions to these interesting regimes

can be achieved in the near future.

Acknowledgments

J.O.S. was supported by a studentship from the Engineering and Physical Sciences Research Council (UK). S.S.K., E.A.E., and A.O.I. gratefully acknowledge research funding from the Russian Science Foundation (Grant No. 15-12-10003). J.O.S., P.J.C., and E.A.E. thank the Ural Federal University for supporting collaborative visits between Edinburgh and Ekaterinburg.

---

[1] R. E. Rosensweig, *Ferrohydrodynamics* (Dover Publications, Inc., New York, 1998).

[2] P. Langevin, J. Phys. Theor. Appl. **4**, 678 (1905).

[3] P. Weiss, J. Phys. Theor. Appl. **6**, 661 (1907).

[4] A. Cebers, Magnetohydrodynamics **18**, 137 (1982).

[5] M. S. Wertheim, J. Chem. Phys. **55**, 4291 (1971).

[6] K. I. Morozov and A. V. Lebedev, J. Mag. Mag. Mater. **85**, 51 (1990).

[7] Yu. A. Buyevich and A. O. Ivanov, Physica A **190**, 276 (1992).

[8] A. O. Ivanov, Magnetohydrodynamics **28**, 353 (1992).

[9] A. F. Pshenichnikov, V. V. Mekhonoshin, and A. V. Lebedev, J. Mag. Mag. Mater. **161**, 94 (1996).

[10] A. O. Ivanov and O. B. Kuznetsova, Phys. Rev. E **64**, 041405 (2001).

[11] A. O. Ivanov and O. B. Kuznetsova, Colloid J. **68**, 430 (2006).

[12] B. Huke and M. Lücke, Phys. Rev. E **62**, 6875 (2000).

[13] B. Huke and M. Lücke, Phys. Rev. E **67**, 051403 (2003).

[14] B. Huke and M. Lücke, Rep. Prog. Phys. **67**, 1731 (2004).

[15] J.-P. Hansen and I. R. McDonald, *Theory of Simple Liquids*, 3rd ed. (Academic Press, London, 2006).

[16] A. O. Ivanov, S. S. Kantorovich, E. N. Reznikov, C. Holm, A. F. Pshenichnikov, A. V. Lebedev, A. Chremos, and P. J. Camp, Phys. Rev. E **75**, 061405 (2007).

[17] A. O. Ivanov, S. S. Kantorovich, E. N. Reznikov, C. Holm, A. F. Pshenichnikov, A. V. Lebedev,

A. Chremos, and P. J. Camp, Magnetohydrodynamics **43**, 393 (2007).

[18] P. J. Camp, E. A. Elfimova, and A. O. Ivanov, J. Phys.: Condens. Matter **26**, 456002 (2014).

[19] A. F. Pshenichnikov and A. V. Lebedev, Sov. Phys. JETP **68**, 498 (1989).

[20] B. H. Erné, K. Butter, B. W. M. Kuipers, and G. J. Vroege, Langmuir **19**, 8218 (2003).

[21] S. H. Chung, A. Hoffmann, S. D. Bader, C. Liu, B. Kay, L. Makowski, and L. Chen, Appl. Phys. Lett. **85**, 2971 (2004).

[22] C. Barrera, V. Florián-Algarin, A. Acevedoa, and C. Rinaldi, Soft Matter **6**, 3662 (2010).

[23] V. L. Calero Diaz del Castillo, D. I. Santiago-Quiñonez, and C. Rinaldi, Soft Matter **7**, 4497 (2011).

[24] R. M. Ferguson, A. P. Khandhar, C. Jonasson, J. Blomgren, C. Johansson, and K. M. Krishnan, IEEE Trans. Magn. **49**, 3441 (2013).

[25] R. S. M. Rikken, R. J. M. Nolte, J. C. Maan, J. C. M. van Hest, D. A. Wilson, and P. C. M. Christianen, Soft Matter **10**, 1295 (2014).

[26] R. E. Rosensweig, J. Magn. Magn. Mater. **252**, 370 (2002).

[27] Q. A. Pankhurst, J. Connolly, S. K. Jones, and J. Dobson, J. Phys. D: Appl. Phys. **36**, R167 (2003).

[28] Q. A. Pankhurst, N. T. K. Thanh, S. K. Jones, and J. Dobson, J. Phys. D: Appl. Phys. **42**, 224001 (2009).

[29] R. Hergt, R. Hiergeist, I. Hilger, W. Kaiser, Y. Lapatnikov, S. Margel, and U. Richter, J. Magn. Magn. Mater. **270**, 345 (2004).

[30] F. Sonvico, S. Mornet, S. Vasseur, C. Dubernet, D. Jaillard, J. Degrouard, J. Hoebeke, E. Duguet, P. Colombo, and P. Couvreur, Bioconjug. Chem. **16**, 1181 (2005).

[31] J.-P. Fortin, C. Wilhelm, J. Servais, C. Ménager, J.-C. Bacri, and F. Gazeau, J. Am. Chem. Soc. **129**, 2628 (2007).

[32] P. Debye, *Polar Molecules* (Chemical Catalog Company, New York, 1929).

[33] H. Fröhlich, *Theory of dielectrics: dielectric constant and dielectric loss*, 2nd ed. (Clarendon Press, Oxford, 1987).

[34] R. Müller, R. Hergt, M. Zeisberger, and W. Gawalek, J. Mag. Magn. Mater. **289**, 13 (2005).

[35] Yu. L. Raikher and V. I. Stepanov, J. Mag. Magn. Mater. **368**, 421 (2014).

[36] M. Boskovic, G. F. Goya, S. Vranjes-Djuric, N. Jovic, B. Jancar, and B. Antic, J. Appl. Phys. **117**, 103903 (2015).

[37] A. Yu. Zubarev and A. V. Yushkov, J. Exp. Theor. Phys. **87**, 484 (1998).

[38] B. U. Felderhof and R. B. Jones, J. Phys.: Condens. Matter **15**, 4011 (2003).

[39] P. Ilg and S. Hess, Z. Naturforsch. **58a**, 589 (2003).

[40] P. M. Déjardin and F. Ladieu, J. Chem. Phys. **140**, 034506 (2014).

[41] E. L. Verde, G. T. Landi, J. A. Gomes, M. H. Sousa, and A. F. Bakuzis, J. Appl. Phys. **111**, 123902 (2012).

[42] M. A. Martens, R. J. Deissler, Y. Wu, L. Bauer, Z. Yao, R. Brown, and M. Griswold, Med. Phys. **40**, 022303 (2013).

[43] G. T. Landi, Phys. Rev. B **89**, 014403 (2014).

[44] A. O. Ivanov, V. S. Zverev, and S. S. Kantorovich, Soft Matter **12**, 3507 (2016).

[45] W. F. Brown, Jr., J. Appl. Phys. **34**, 1319 (1963).

[46] W. F. Brown, Jr., IEEE Trans. Magn. **15**, 1196 (1979).

[47] "LAMMPS Molecular Dynamics Simulator," (1995), http://lammps.sandia.gov.

[48] S. Plimpton, J. Comp. Phys. **117**, 1 (1995).

[49] J. J. Weis and D. Levesque, Phys. Rev. Lett. **71**, 2729 (1993).

[50] L. Rovigatti, J. Russo, and F. Sciortino, Soft Matter **8**, 6310 (2012).

[51] S. Kantorovich, A. O. Ivanov, L. Rovigatti, J. M. Tavares, and F. Sciortino, Phys. Rev. Lett. **110**, 148306 (2013).

TABLE I: System parameters and results from BD simulations: ρ^* is the reduced concentration; λ is the dipolar coupling constant; $\chi_{\rm L} = 4\pi\rho^*\lambda/3$ is the Langevin susceptibility; $\chi(0)$ is the static susceptibility; ω_0 is the peak frequency in $\chi''(\omega)$; τ_0 is the characteristic decay time of the MACF; A and B are the initial low-frequency slopes of $\chi'(\omega^2)/\chi(0)$ and $\chi''(\omega)$, respectively, relative to the Debye-theory values; $\tau_{\rm B}$ is the Brownian rotation time; and N is the number of particles. All results are quoted to three significant figures, and all of the fitting errors are zero at this level of precision.

$\rho^* = 0.20$							$\lambda = 1$					
$\chi_{\rm L}$	λ	$\chi(0)$	$\omega_0\tau_{\rm B}$	$\tau_0/\tau_{\rm B}$	A	B	ρ^*	$\chi(0)$	$\omega_0\tau_{\rm B}$	$\tau_0/\tau_{\rm B}$	A	B	N
0.209	0.25	0.217	0.971	1.04	1.06	1.08							216
0.419	0.50	0.466	0.888	1.14	1.32	1.27	0.10	0.463	0.876	1.17	1.39	1.29	216
0.628	0.75	0.746	0.824	1.20	1.40	1.43							216
0.838	1.00	1.06	0.741	1.34	1.77	1.70	0.20	1.06	0.747	1.34	1.78	1.69	216
1.05	1.25	1.40	0.689	1.42	1.93	1.90							216
1.26	1.50	1.78	0.625	1.66	2.93	2.35	0.30	1.77	0.668	1.49	2.17	2.10	216
1.47	1.75	2.22	0.554	1.78	3.10	2.70							216
1.68	2.00	2.68	0.503	2.08	4.75	3.33	0.40	2.58	0.598	1.64	2.57	2.53	216
2.09	2.50	3.85	0.375	2.60	6.66	4.78	0.50	3.51	0.552	1.81	3.25	3.03	216
2.51	3.00	5.41	0.265	3.70	13.6	7.97	0.60	4.58	0.508	1.96	3.75	3.56	216
		5.38	0.272	3.57	12.7	7.65		4.62	0.508	1.97	3.90	3.62	512
2.93	3.50	7.28	0.188	5.04	24.3	12.5	0.70	5.88	0.463	2.17	4.68	4.35	216
		7.40	0.180	5.28	26.9	13.3		5.91	0.456	2.32	5.96	4.68	512

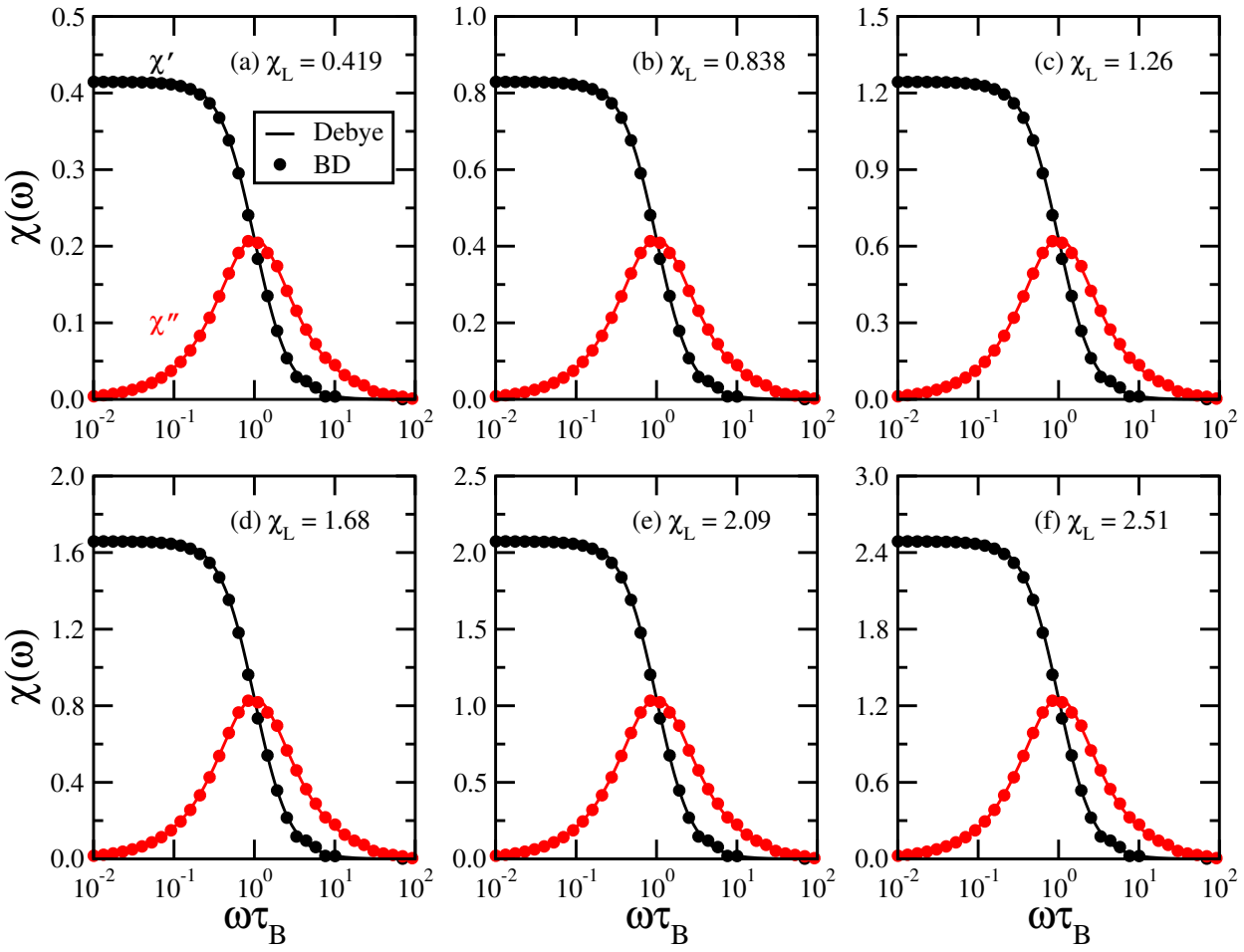

FIG. 1: The susceptibility spectra $\chi(\omega)$ of systems at $\rho^* = 0.20$ and with the dipole-dipole interactions turned off ($u_{ij}^{\rm d} = 0$). The points are from simulations with $N = 216$ particles, and the lines are from Debye theory [Eq. (11)]. The system parameters are: (a) $\lambda = 0.50$, $\chi_{\rm L} = 0.419$; (b) $\lambda = 1.00$, $\chi_{\rm L} = 0.838$; (c) $\lambda = 1.50$, $\chi_{\rm L} = 1.26$; (d) $\lambda = 2.00$, $\chi_{\rm L} = 1.68$; (e) $\lambda = 2.50$, $\chi_{\rm L} = 2.09$; (f) $\lambda = 3.00$, $\chi_{\rm L} = 2.51$. For clarity, only 1-in-20 simulation points are shown.

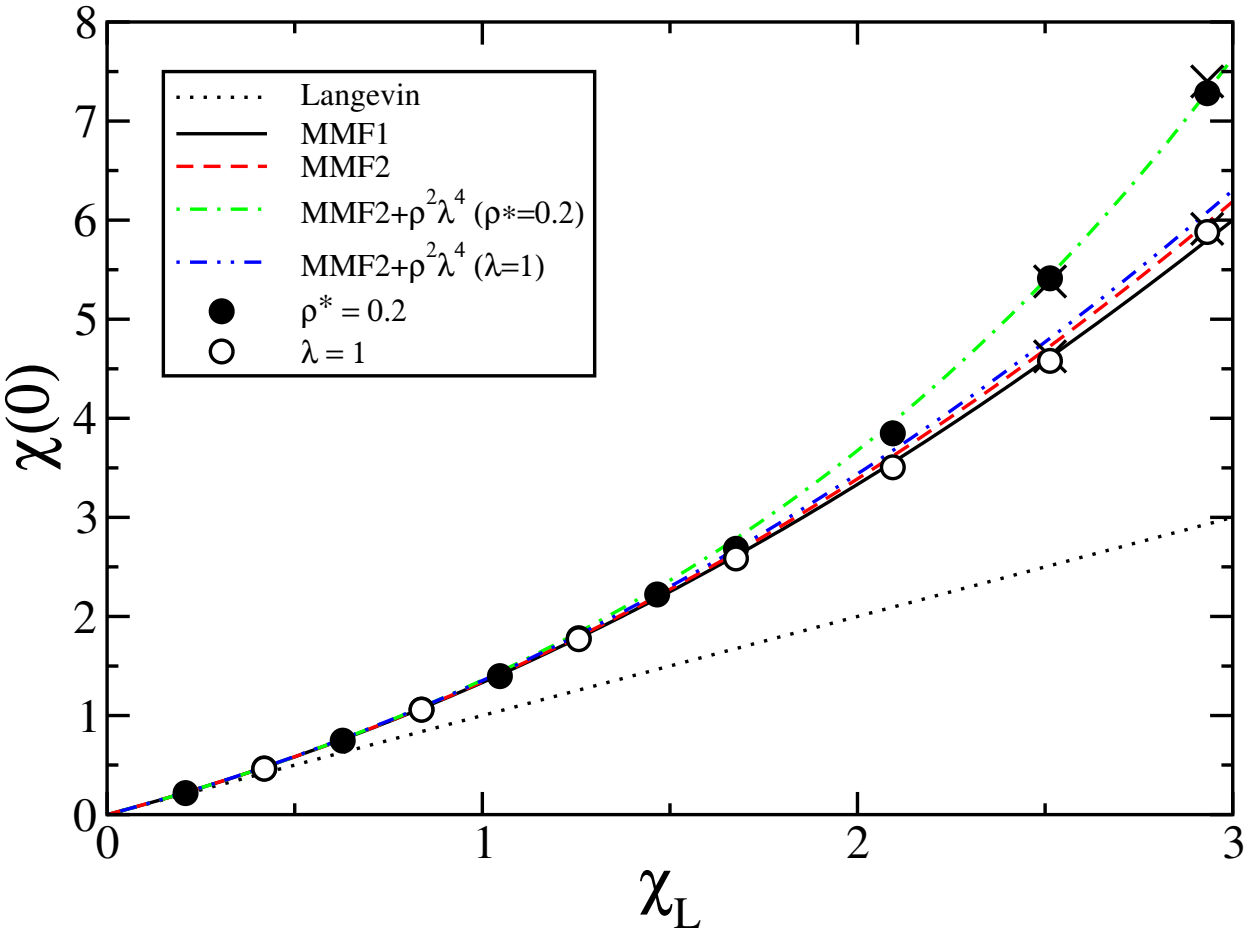

FIG. 2: The static susceptibility as a function of the Langevin susceptibility. The points are from simulations with $N = 216$ particles at $\rho^* = 0.2$ (filled circles) and $\lambda = 1$ (unfilled circles); the crosses are for systems with $N = 512$ particles. The lines are from various theories: Langevin [Eq. (10)] – dotted black line; MMF1 [Eq. (16)] – solid black line; MMF2 [Eq. (28)] – red dashed line; MMF2 $+ \rho^2\lambda^4$ [Eq. (29)] at $\rho^* = 0.2$ – green dot-dashed line; MMF2 $+ \rho^2\lambda^4$ with $\lambda = 1$ – blue dot-dot-dashed line.

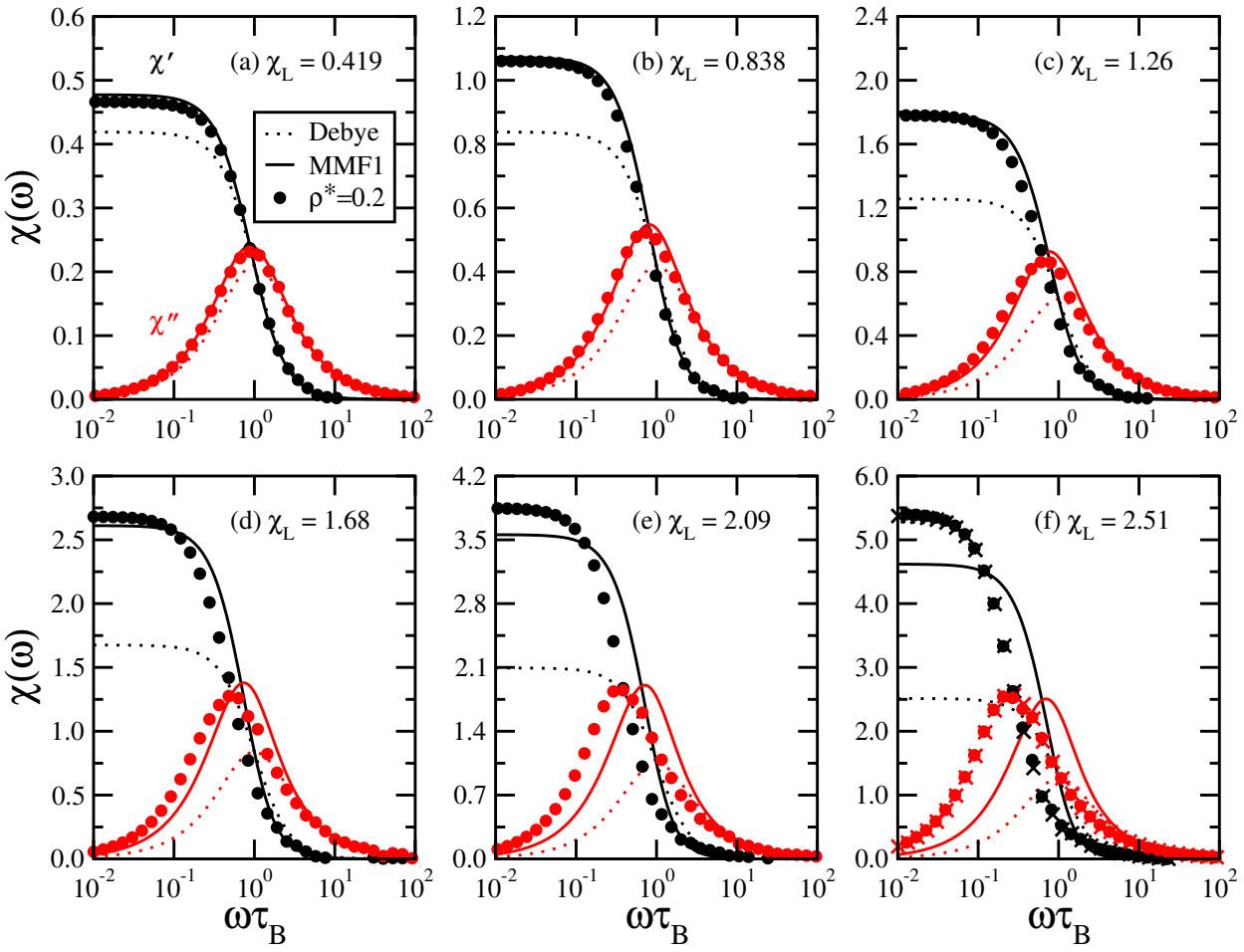

FIG. 3: The susceptibility spectra $\chi(\omega)$ of interacting particles at $\rho^* = 0.20$. The points are from simulations with $N = 216$ particles, the crosses in (f) are from simulations with $N = 512$ particles, the dotted lines are from Debye theory [Eq. (11)], and the solid lines are from MMF1 theory [Eq. (15)]. The system parameters are: (a) $\lambda = 0.50$, $\chi_L = 0.419$; (b) $\lambda = 1.00$, $\chi_L = 0.838$; (c) $\lambda = 1.50$, $\chi_L = 1.26$; (d) $\lambda = 2.00$, $\chi_L = 1.68$; (e) $\lambda = 2.50$, $\chi_L = 2.09$; (f) $\lambda = 3.00$, $\chi_L = 2.51$. For clarity, only 1-in-20 simulation points are shown.

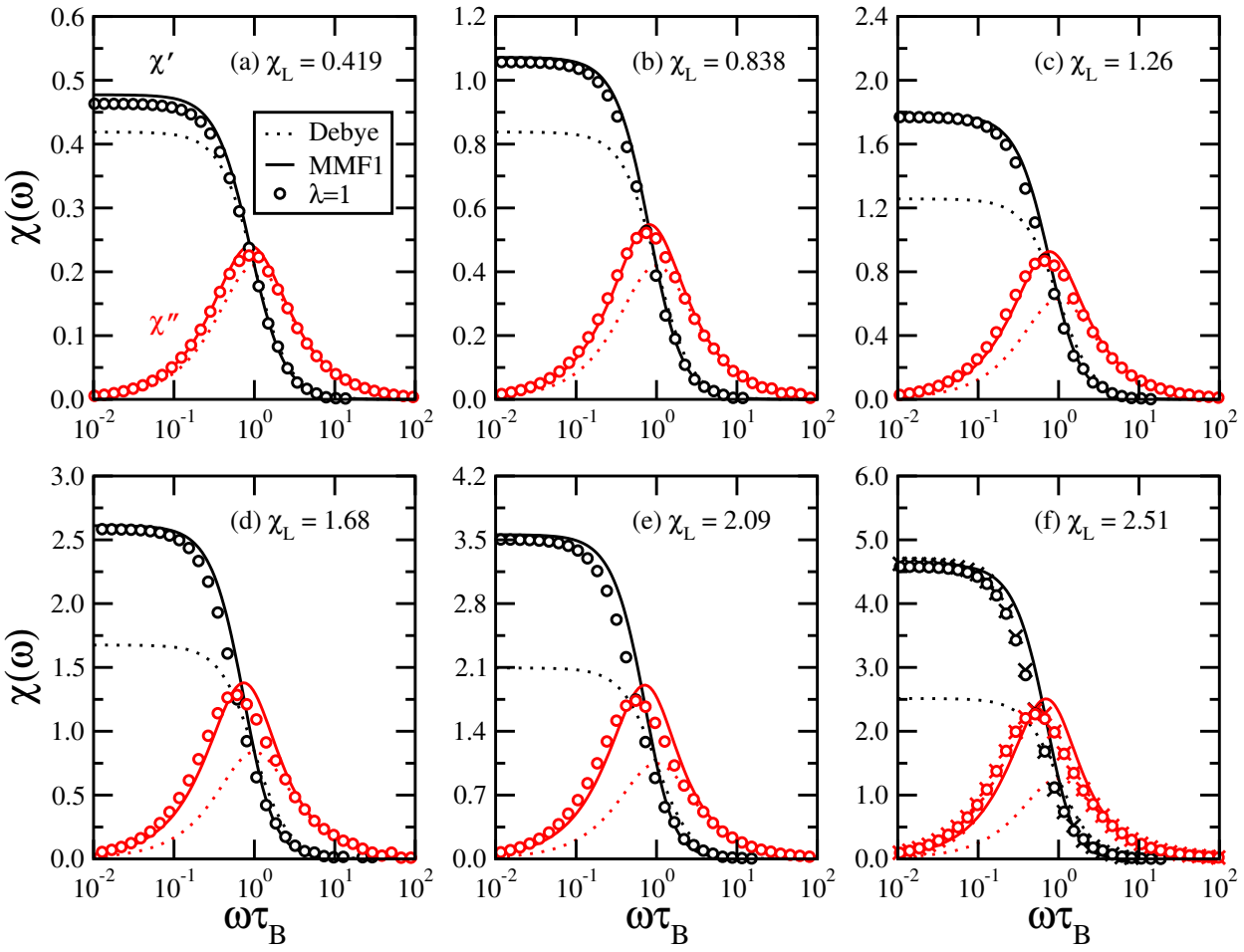

FIG. 4: The susceptibility spectra $\chi(\omega)$ of interacting particles with $\lambda = 1$. The points are from simulations with $N = 216$ particles, the crosses in (f) are from simulations with $N = 512$ particles, the dotted lines are from Debye theory [Eq. (11)], and the solid lines are from MMF1 theory [Eq. (15)]. The system parameters are: (a) $\rho^* = 0.10$, $\chi_L = 0.419$; (b) $\rho^* = 0.20$, $\chi_L = 0.838$; (c) $\rho^* = 0.30$, $\chi_L = 1.26$; (d) $\rho^* = 0.40$, $\chi_L = 1.68$; (e) $\rho^* = 0.50$, $\chi_L = 2.09$; (f) $\rho^* = 0.60$, $\chi_L = 2.51$. For clarity, only 1-in-20 simulation points are shown.

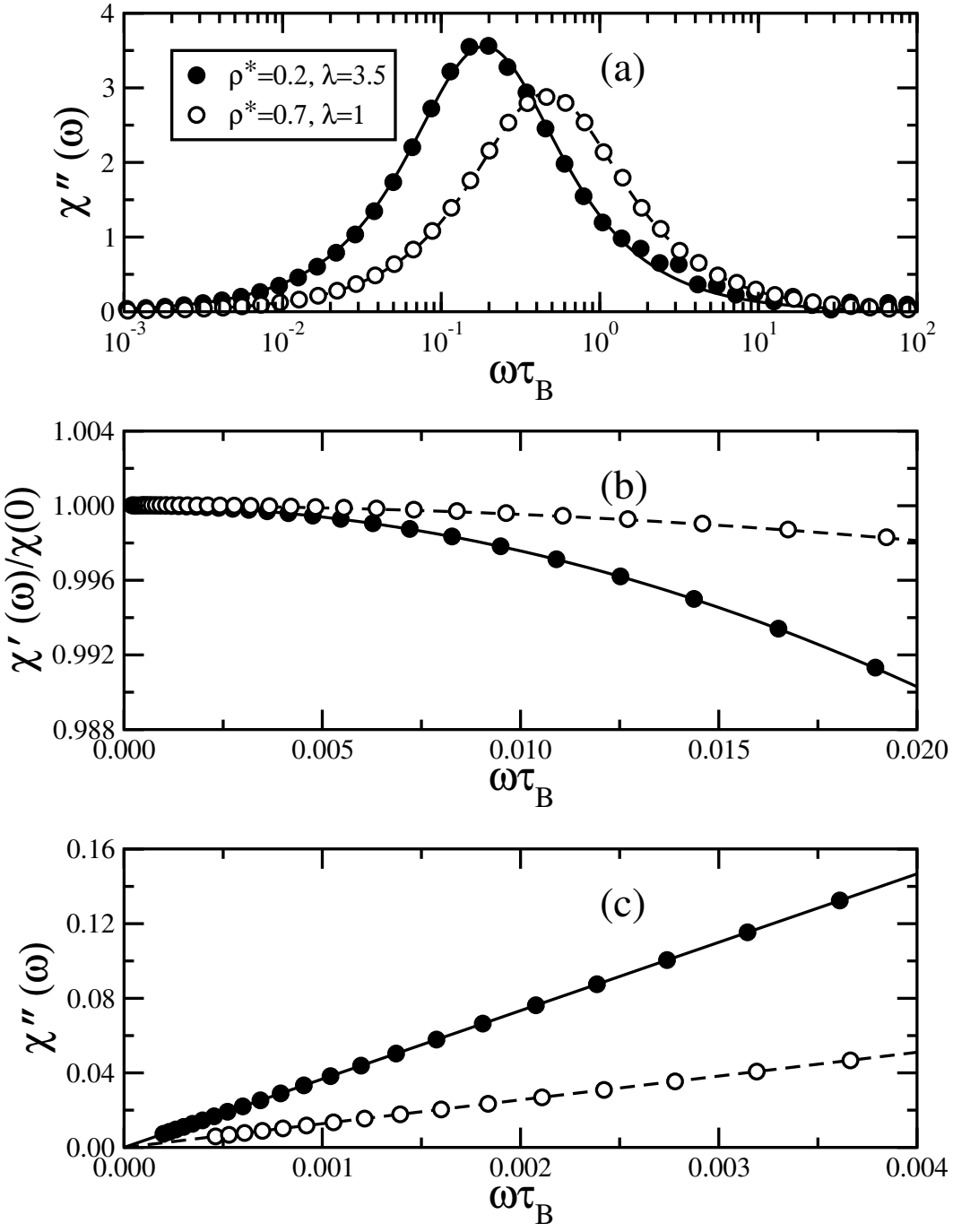

FIG. 5: Examples of fits to extract the parameters ω_0, A, and B from the susceptibility spectra of systems with $N = 216$ particles and $\chi_{\rm L} = 2.93$: $\rho^* = 0.20$ and $\lambda = 3.50$ (filled circles and solid lines); $\rho^* = 0.70$ and $\lambda = 1$ (unfilled circles and dashed lines). (a) $\chi''(\omega)$ near the peak frequency fitted with an equation of the same form as $\chi''_{\rm D}(\omega)$ [Eq. (11c)]. (b) Low-frequency portion of $\chi'(\omega)/\chi(0)$ fitted with Eq. (18). (c) Low-frequency portion of $\chi''(\omega)$ fitted with Eq. (19). For clarity, only 1-in-20 simulation points are shown in (a), and 1-in-10 in (b) and (c).

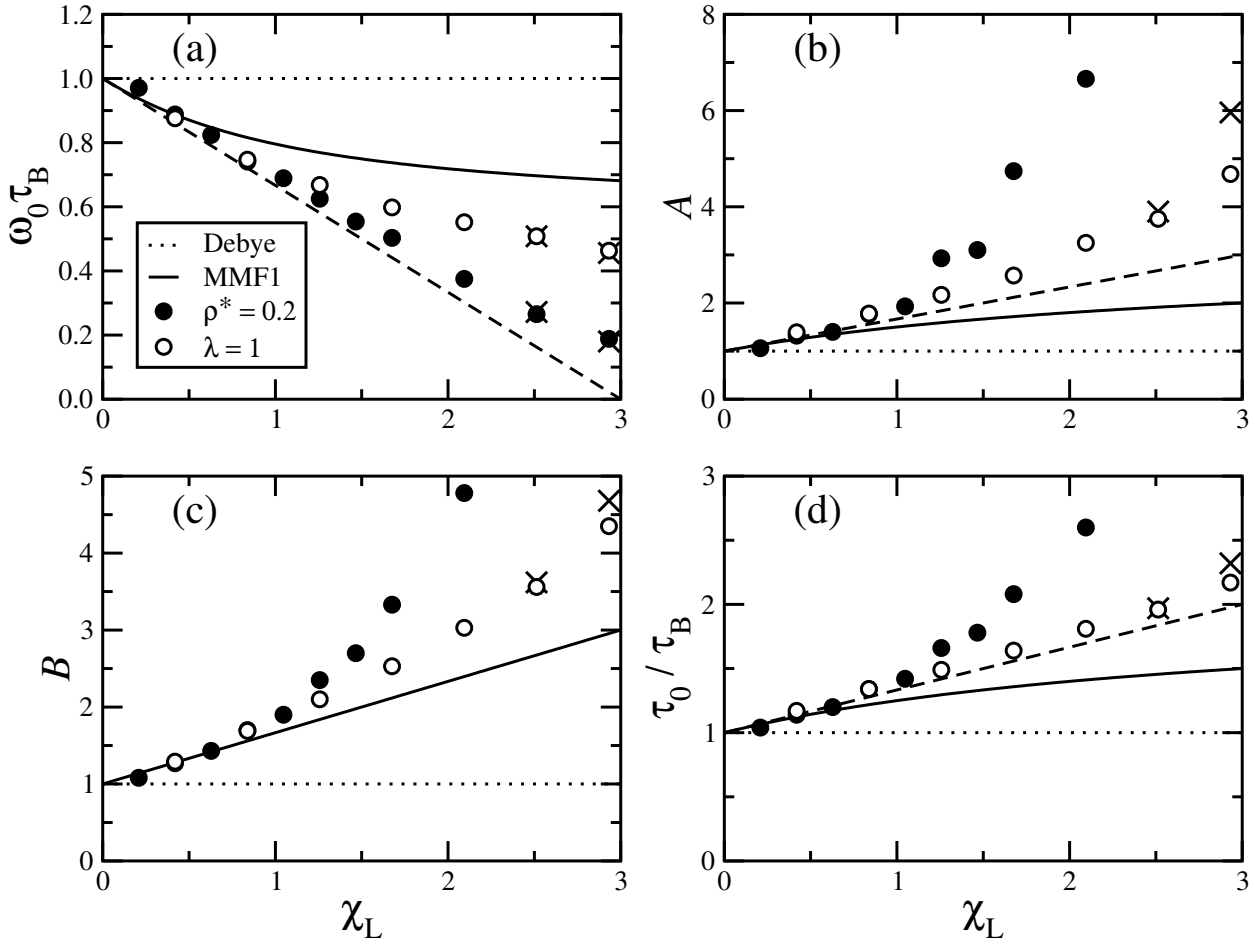

FIG. 6: Fit parameters from the susceptibility spectra of systems with $N = 216$ particles simulated at $\rho^* = 0.20$ (filled circles) and with dipolar coupling constant $\lambda = 1$ (unfilled circles); the crosses are from simulations with $N = 512$ particles. The theoretical predictions are from Debye theory (dotted lines), MMF1 theory (solid lines), and the initial linear extrapolation of MMF1 (dashed lines). (a) Peak frequency ω_0 in $\chi''(\omega)$. (b) Coefficient A in Eq. (18). (c) Coefficient B in Eq. (19). (d) Characteristic decay time τ_0 of the MACF in Eq. (26).

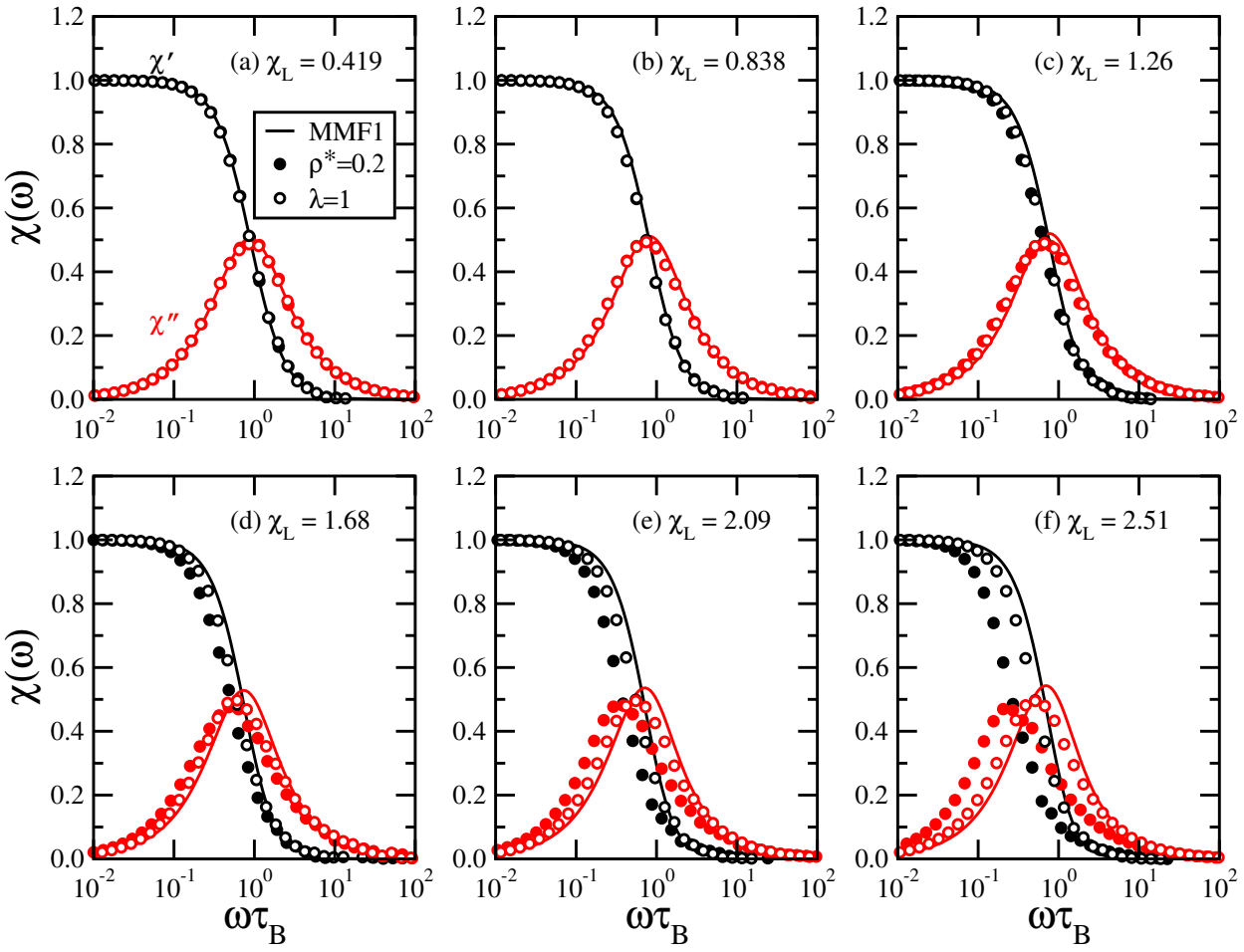

FIG. 7: Normalized susceptibility spectra $\chi(\omega)$ of interacting particles at $\rho^* = 0.20$ and with $0.50 \leq \lambda \leq 3.00$ (filled circles), at $0.10 \leq \rho^* \leq 0.60$ and with $\lambda = 1$ (unfilled circles), and from MMF1 theory (solid lines). All simulation points are from systems with $N = 216$ particles. The Langevin susceptibilities are: (a) $\chi_L = 0.419$; (b) $\chi_L = 0.838$; (c) $\chi_L = 1.26$; (d) $\chi_L = 1.68$; (e) $\chi_L = 2.09$; (f) $\chi_L = 2.51$. For clarity, only 1-in-20 simulation points are shown.